Electronic Supplementary Material (ESI) for Sustainable Energy & Fuels.

Supplementary Information

Permselective ion electrosorption of subnanometer pores at high molar strength enables capacitive deionization of saline water

Sheng Bi,[1,2,+] Yuan Zhang,[3,4,+] Luca Cervini,[5] Tangming Mo,[1,2]
John M. Griffin,[5,6] Volker Presser,[3,4,*] Guang Feng[1,2,*]

[1] State Key Laboratory of Coal Combustion, School of Energy and Power Engineering, Huazhong University of Science and Technology (HUST), Wuhan 430074, China.

[2] Nano Interface Centre for Energy, School of Energy and Power Engineering, HUST, 430074, China.

[3] INM - Leibniz Institute for New Materials, Campus D2 2, 66123 Saarbrücken, Germany.

[4] Department of Materials Science and Engineering, Saarland University, Campus D2 2, 66123 Saarbrücken, Germany.

[5] Department of Chemistry, Lancaster University, Lancaster, LA1 4YB, United Kingdom.

[6] Materials Science Institute, Lancaster University, Lancaster, LA1 4YB, United Kingdom.

[+] These authors contributed equally: Bi Sheng, Yuan Zhang.

[*] Corresponding authors. Email: volker.presser@leibniz-inm.de (VP); gfeng@hust.edu.cn (GF)

1. Data for the molecular dynamics simulation setup

Table S1. The number of ion pairs ($n_{ion\ pair}$) and water molecules (n_{water}) in each molecular dynamics (MD) simulation system.

Pore size (nm)	$n_{ion\ pair}$	n_{water}
0.42	163	4522
0.44	168	4661
0.47	171	4732
0.5	172	4788
0.53	174	4836
0.57	178	4953
0.59	180	4991
0.62	181	5040
0.65	185	5150
0.77	197	5469
0.97	212	5892
1.17	230	6401
1.37	246	6818
1.57	263	7300
1.77	278	7735

2. Characterization of carbons and cell setup

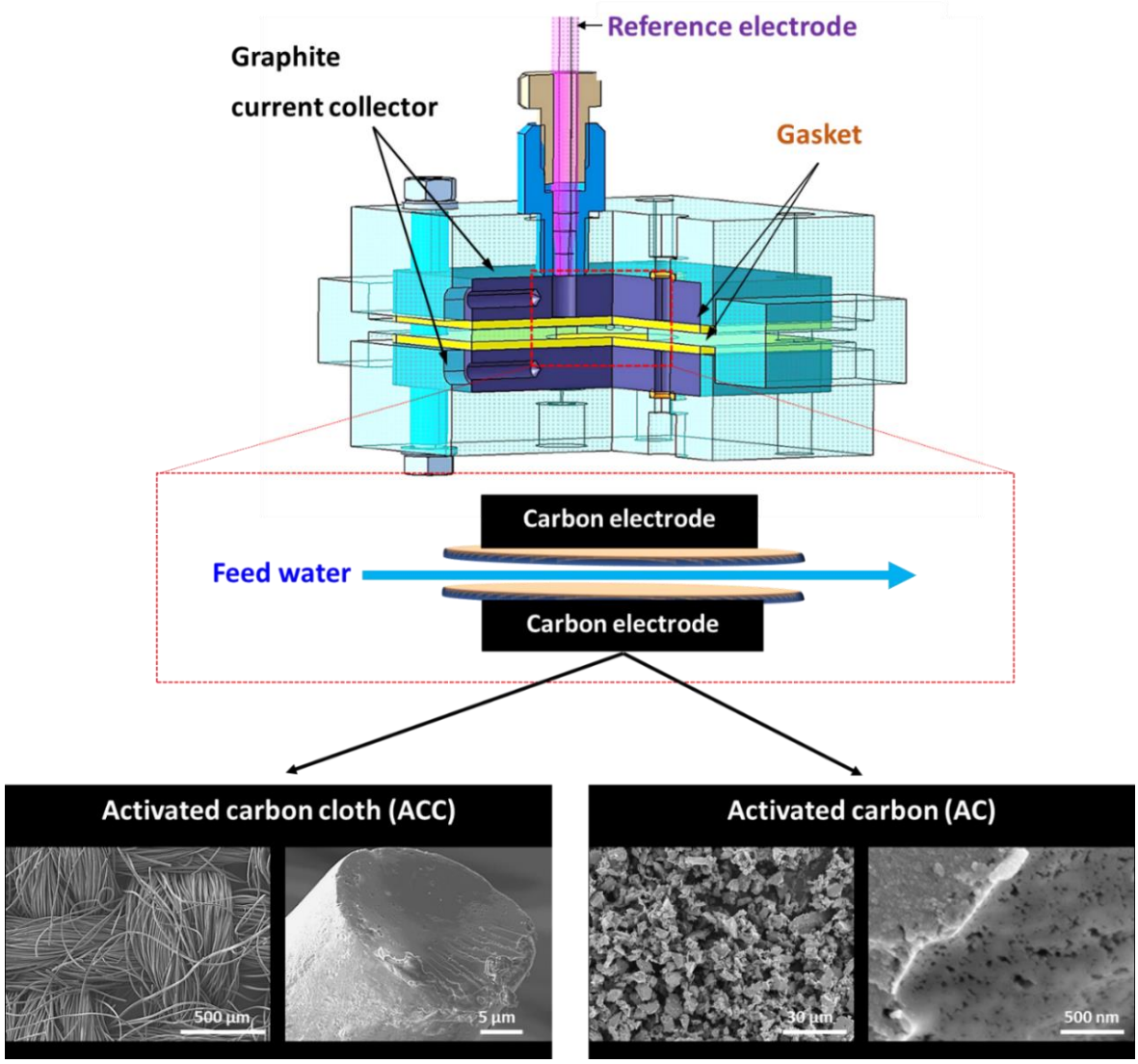

Figure S1. Schematic view of the CDI cell and scanning electron micrographs of carbon electrode materials.

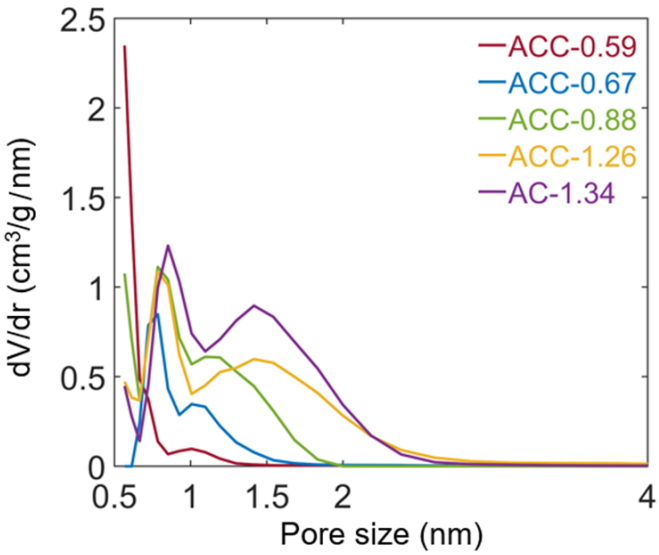

Figure S2. Differential pore size distribution. Data are obtained from nitrogen gas sorption isotherms at -196 °C, calculated by applying quenched solid density functional theory (QSDFT) and assuming pores have slit shape.

Table S2. Specific surface area (BET and DFT), total pore volume, and volume-weighted pore size of ACC-0.59, ACC-0.67, ACC-0.88, ACC-1.26, and AC-1.34.

	SSA BET (m^2/g)	SSA DFT (m^2/g)	Pore volume (cm^3/g)	d_{25} (nm)	d_{50} (nm)	d_{75} (nm)	d_{75}-d_{25} (nm)
ACC-0.59	916	1032	0.34	0.55	0.59	0.68	0.12
ACC-0.67	1478	1550	0.56	0.45	0.67	0.86	0.41
ACC-0.88	2070	1876	0.81	0.64	0.88	1.19	0.55
ACC-1.26	2794	2191	1.22	0.89	1.26	1.61	0.72
AC-1.34	2104	1756	1.00	0.86	1.34	1.80	0.94

Table S3. CHN-O elemental analysis of ACC-0.59, ACC-0.67, ACC-0.88, ACC-1.26, and AC-1.34 (unit: mass%). "n.d." demarks values below the detection limit of the system ("not detectable").

	C	H	N	O
ACC-0.59	>94	n.d.	<1	<6
ACC-0.67	>96	<1	<0.1	<2
ACC-0.88	>96	<2	<0.2	<2
ACC-1.26	>96	<1	n.d	<3
AC-1.34	>95	<1	n.d	<4

3. Desalination performance measurements with aqueous NaCl solution

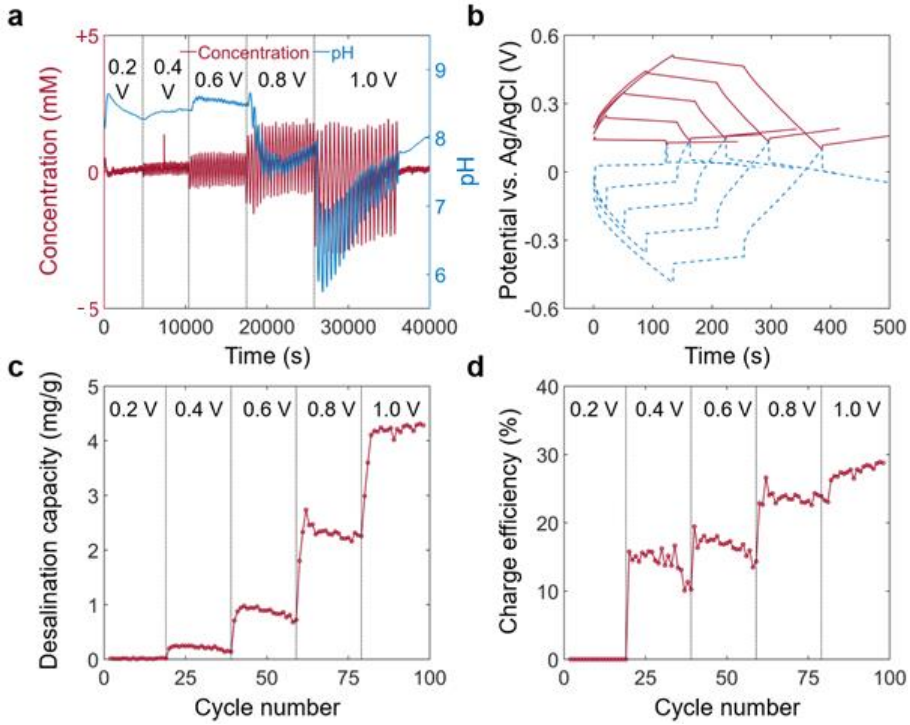

Figure S3. CDI measurement for ACC-0.59 carbon cloth in 800 mM NaCl. a, Concentration change (relative to 800 mM) and pH profile. **b,** Galvanostatic charging and discharging for the working electrode (red line) and counter electrode (blue dash line). **c-d,** Desalination capacity (**c**) and charge efficiency (**d**) profile at each cycle.

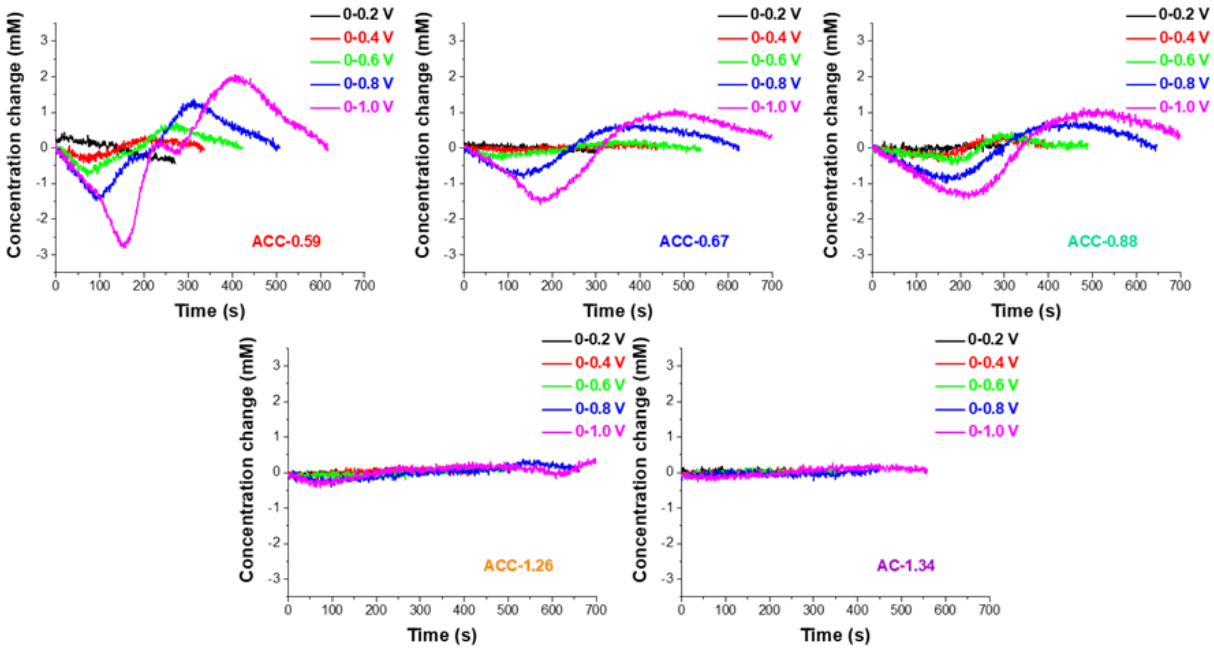

Figure S4. Representative concentration change pattern for different carbon electrode materials in 800 mM NaCl.

4. Basic electrochemical characterization

To determine the basic electrochemical properties of ACC electrodes in 2 M KCl system, half-cell characterization was carried out with a custom-built cell using spring-loaded titanium pistons. To assemble the cell, a 12 mm diameter disk of the ACC electrode material (around 20 mg) was cut and employed as the working electrode. 13 mm diameter of glass fiber mat (GF/A, Whatman) was employed as the separator. As for the counter-electrode, a free-standing YP-80F/PTFE 95:5 electrode (thickness: 650 µm) was used. 12 mm diameter of graphite foil was applied as current collectors. The aqueous 2 M KCl solution was inserted into the cell by vacuum filling with a syringe, and an Ag/AgCl reference electrode (3 M KCl, BASi) was located at the side of the cell body and assembled close to working electrode and counter electrode. The cell was characterized by using VSP300 potentiostat/galvanostat (Bio-Logic). For cyclic voltammetry, the cell was cycled between -0.5 V and +0.5 V vs. Ag/AgCl at the scan rate of 1 mV/s. For galvanostatic charge/discharge, the specific current of 0.1 A/g was applied to the electrode with potential applied from 0 V vs. Ag/AgCl to the cut-off potentials of +0.2 V, +0.4 V, +0.6 V, +0.8 V, and +1.0 V vs. Ag/AgCl (ten cycles for each potential range). The specific capacitance of the electrode is calculated according to **Eq. S1**.

$$C_{specific} = \frac{1}{Um}\int_{t_1}^{t_2} Idt \qquad \textbf{(Eq. S1)}$$

where *U* is the voltage difference during the discharge process (excluding the Ohmic drop), *m* is mass of the working electrode, t_2-t_1 is the discharge time interval, and *I* is the applied discharge current.

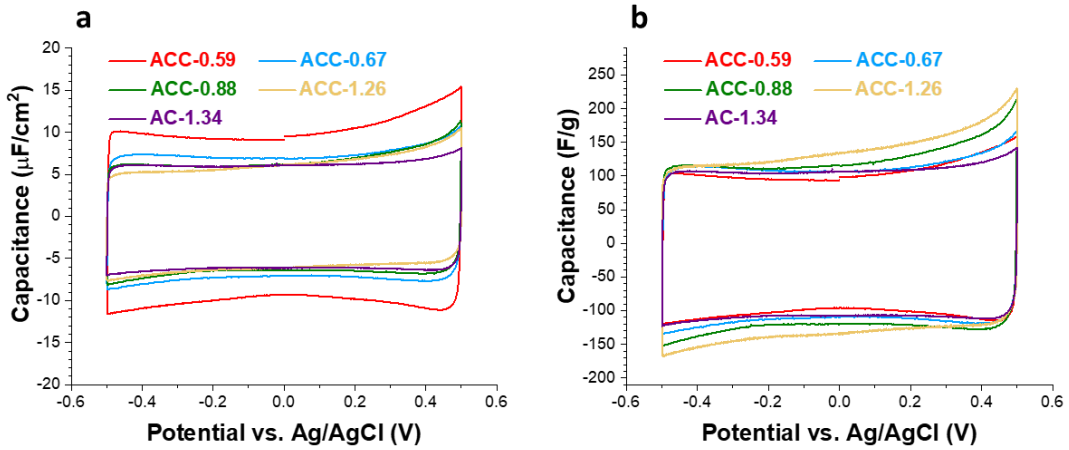

Figure S5. Cyclic voltammogram measurements. Performed at 1 mV/s for five carbon electrodes in 2 M KCl water solution. ACC and AC carbons are applied as working electrodes, and YP-80F+5% PTFE electrodes are applied as counter electrodes. **a**, normalized to specific surface area; **b**, normalized to electrode mass.

5. In-pore ions under different polarizations

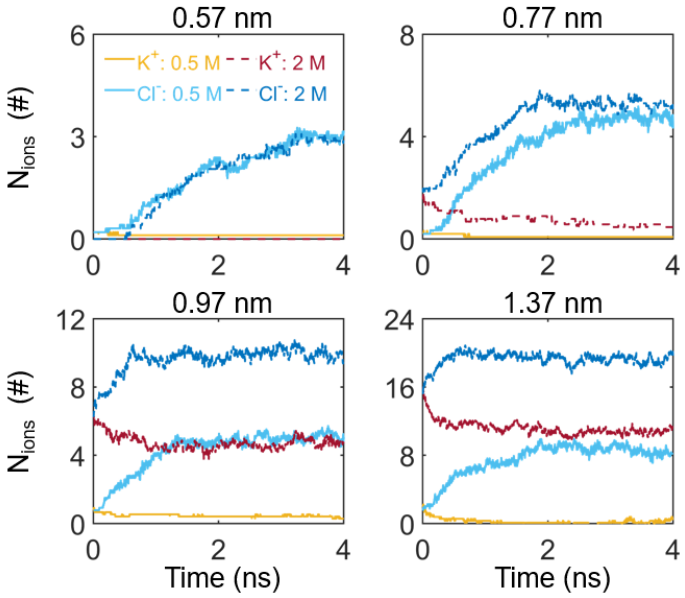

Figure S6. Time evolution of the number of cation and anion in the positively charged micropores. The applied voltage between the positive and negative electrode is set to 1.0 V. Dark red and blue solid lines are, respectively, results for the cation and anion at 2 M concentration. Yellow and light blue dashed lines are for cation and anion at 0.5 M concentration. These results are evaluated on-the-fly during the charging simulations of each micropore.

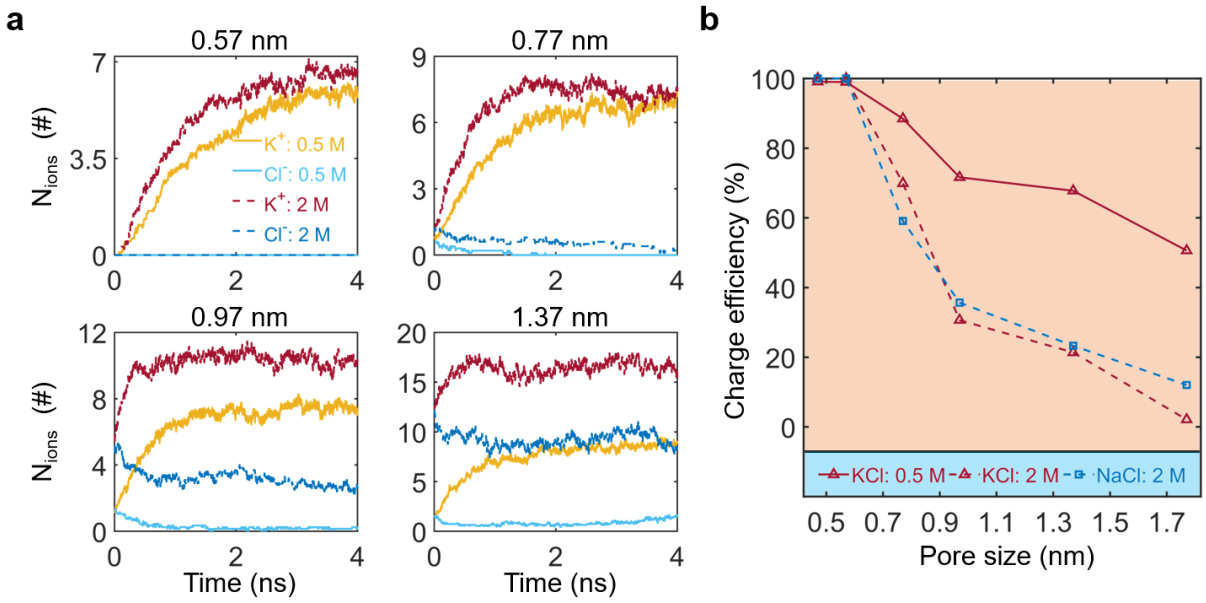

Figure S7. Molecular understanding of ion permselectivity by micropores at 1.5 V. a, Time evolution of the number of cation and anion in the negatively charged micropores. Dark red and blue solid lines are, respectively, results for the cation and anion at 2 M. Yellow and light blue dashed lines are for cation and anion at 0.5 M. These results are evaluated during the charging simulations of each micropore. **b,** Charge efficiency, as a function of pore size. Red solid and dashed lines with triangle markers represent results of micropores in aqueous 0.5 M and 2 M KCl solutions, respectively. Blue dashed line with squares: 2 M NaCl solution.

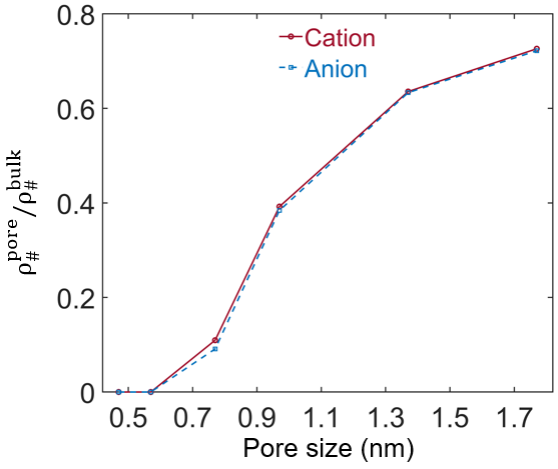

Figure S8. Normalized in-pore ion density at PZC. The in-pore ion density is scaled by bulk ion density. Solid and dash lines are, respectively, for the cation and anion at 2 M.

6. Water distribution surrounding ions in bulk and inside large pores

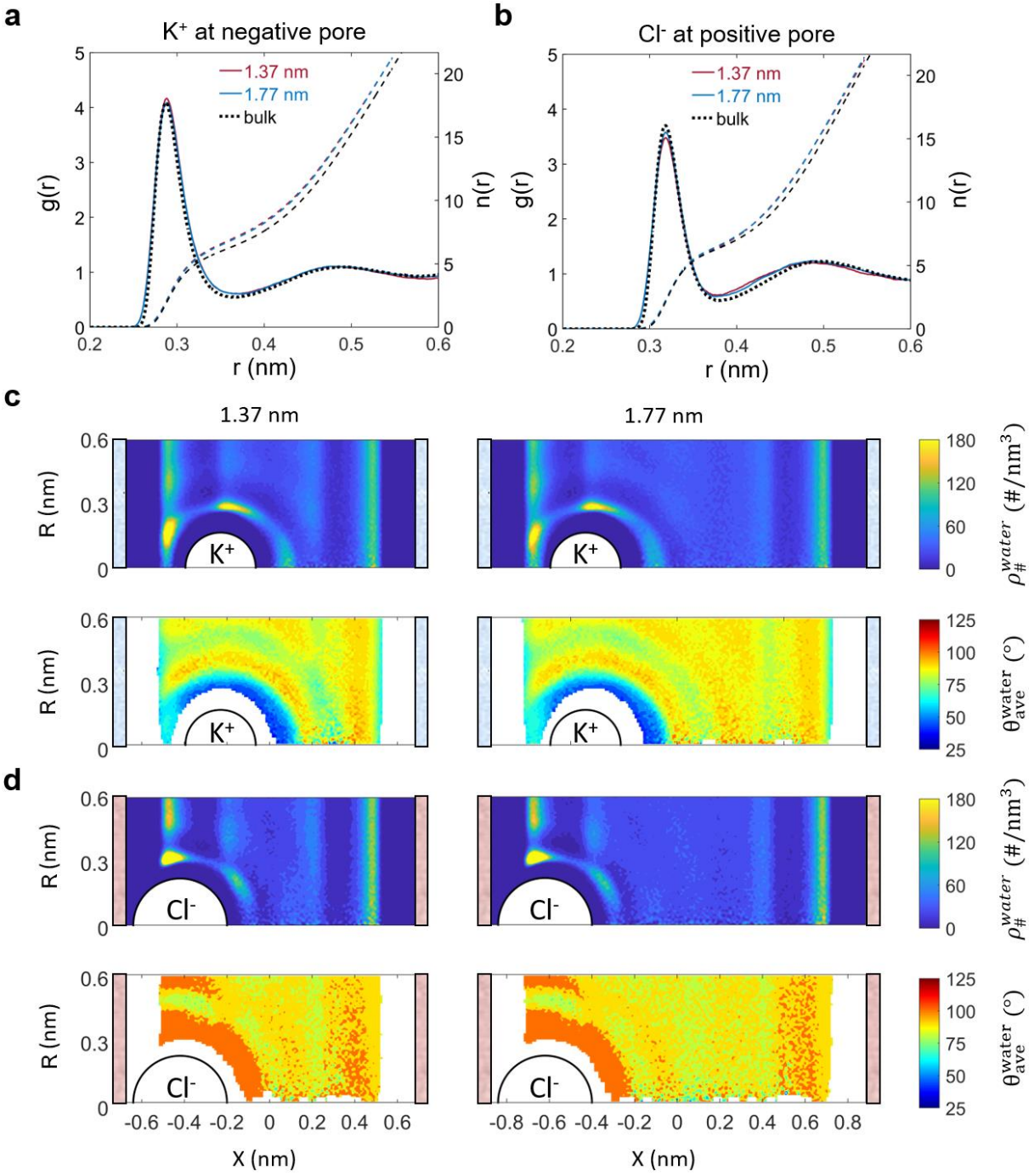

Figure S9. Structure of hydration shells of counter-ions in >1 nm polarized micropores. a-b, Radial distribution function, g(r) (solid lines, left Y-axis), and cumulative distribution function, n(r) (dashed, right Y-axis) of hydrated K^+ ions (left panel) and Cl^- ions (right panel) in negatively and positively polarized pores, respectively. Black dot lines are results for ions in bulk simulations. **c-d,** Pseudo-2D number density distributions and orientations of water molecules around an ion in micropores of 1.37 nm and 1.77 nm; the upper two rows and the lower two are results (first number density, then orientation distributions) for water around a K^+ ion under negative polarization and for water around a Cl^- ion under positive polarization, respectively. X = 0 corresponds to the central position of the pore.

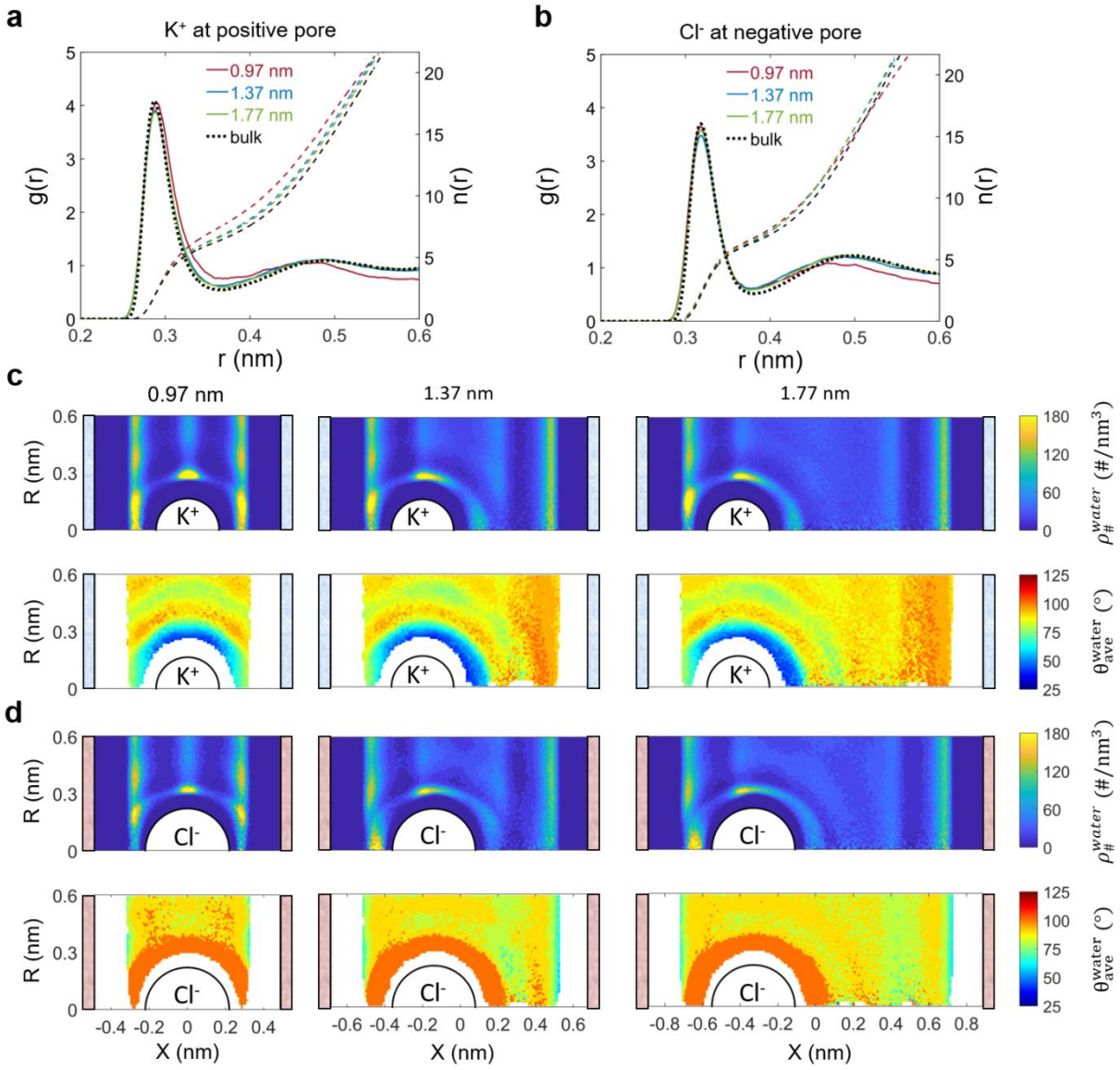

Figure S10. Structure of hydration shells of co-ions in polarized micropores. a-b, Radial distribution function, g(r) (solid lines, left Y-axis), and cumulative distribution function, n(r) (dashed, right Y-axis) of hydrated K^+ ions (left panel) and Cl^- ions (right panel) in positively and negatively polarized pores, respectively. Black dot lines are results for ions in bulk simulations. **c-d,** Pseudo-2D number density (upper panel) and orientation (lower panel) distributions of water molecules around a co-ion in micropores of different pore sizes under positive and negative polarizations, respectively. We show K^+ ion (**c**) in positively charged pores and Cl^- ion (**d**) in negatively charged pores. X = 0 corresponds to the central position of the pore.

7. Dynamics of ions inside charged pores

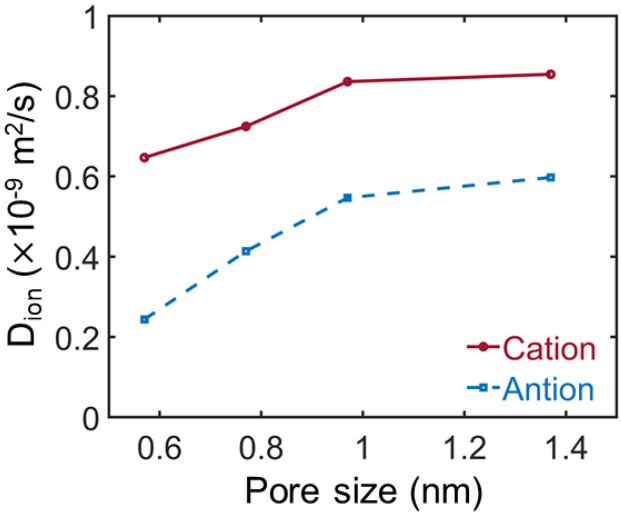

Figure S11. In-pore ion diffusion. Self-diffusion coefficients of cations and anions in negatively and positively charged pores, respectively. The voltage applied between the positive and negative electrode is set at 1.0 V.